Journal of Magnetism and Magnetic Materials 339 (2013) 75–80

Contents lists available at SciVerse ScienceDirect

Journal of Magnetism and Magnetic Materials

journal homepage: www.elsevier.com/locate/jmmm

Properties of $Fe_{8-N}Co_N$ nanoribbons and nanowires: A DFT approach

Francisco Muñoz [a,b,c], D. Altbir [c,d], Miguel Kiwi [b,c,*], J.L. Morán-López [e]

[a] Max Planck Institute of Microstructure Physics, Weinberg 2, 06120 Halle, Germany
[b] Departamento de Física, Facultad de Ciencias, Universidad de Chile, Casilla 653, Santiago 7800024, Chile
[c] Centro para el Desarrollo de la Nanociencia y la Nanotecnología, CEDENNA, Avda. Ecuador 3493, Santiago 9170124, Chile
[d] Departamento de Física, Universidad de Santiago, Chile
[e] Departamento de Física, Laboratorio Interdisciplinario, Facultad de Ciencias, Universidad Nacional Autónoma de México, México, D.F., Mexico

ARTICLE INFO

Article history:
Received 7 November 2012
Received in revised form
10 February 2013
Available online 5 March 2013

Keywords:
Structure of nanowire
Magnetic property of nanostructure
Ab initio calculation

ABSTRACT

The structural configurations and magnetic properties of zig-zag nanoribbons and nanowires of $Fe_{8-N}Co_N$, for $0 \le N \le 8$, are calculated within the density functional theory. Both, for the zig-zag nanoribbons and the nanowires, there is a tendency towards forming Fe–Co bonds, while segregation of the Fe and Co is energetically unfavorable. For the nanowire structures a transition from bcc Fe to hcp Co spatial arrangements is observed when N is increased from 4 to 6, in spite of the small size of the systems under investigation. The energy minimization was performed taking into consideration the electronic and magnetic structures, since for each crystalline structure, chemical composition, and short range order, particular magnetic properties of these systems do correspond. The magnetocrystalline anisotropy energy is calculated, and it is found that the easy axis changes from a transverse direction in Fe-rich systems, to the axial direction as the Co concentration increases. It is also found that although there are important variations of the local magnetic moment of the components, and their particular location in the system, the average magnetic moment is an almost linear function of N.

1. Introduction

Arrays of cylindrically shaped magnetic nanostructures like rods, pillars, tubes and wires, have attracted much attention lately due to their interesting physical properties, as well as their potential for applications as patterned magnetic recording media [1]. Physical properties of these arrays, such as the underlying crystalline structure, the magnetization, and the magnetic anisotropies can be strongly affected by several factors like the size, synthesis process, the constituent elements and their relative concentration.

Different lithographic techniques have been used to grow large arrays of these elements [2], usually of uniform shape and sizes. In these media, the magnetic behavior is determined both by the magnetic characteristics of individual nanoparticles, as well as the strength of the inter-element magnetostatic interactions. However, and in spite of the many advantages that lithography has, like the possibility of printing regular arrays over large areas, it is expensive and time consuming. Alternatively, chemical template-based methods combined with high-yield electrochemical deposition techniques have been used to construct arrays of magnetic nanoribbons and nanowires [3]. A common method is based on the preparation of self-assembled nanoporous anodic alumina membranes fabricated by a two-step anodization process [4,5]. After preparing the alumina template, the pores can be filled electrochemically, and the amount of material can be controlled through the charge recorded during the growth of the elements [6].

Among the properties that make magnetic materials technologically important the most relevant are the magnetocrystalline anisotropy and the magnetization density. While the latter is determined mainly by the constituents and the crystallography, the former is strongly influenced by shape. Due to the strong shape anisotropy of wires and tubes, the easy axis is in general parallel to the cylinder axis. However, it has been shown that the crystalline anisotropy plays a fundamental role and, depending on the material, it can overcome the dipole contribution and lead to a perpendicular easy axis orientation. This effect may be more important for alloy nanowires than for pure element nanowires, since the easy axis points along parallel and perpendicular directions, respectively.

In the case of FeCo nanowires, Pierce et al. [7], observed significant changes in the Curie temperature, as a function of the relative concentration of Fe and Co. In these alloys the structure changes from bcc, for low Co concentrations, to a mixture of both bcc and fcc structures for large Co concentrations. Furthermore, Burkert et al. [8] suggested that tetragonal Fe_NCo_M

* Corresponding author at: Departamento de Física, Facultad de Ciencias, Universidad de Chile, Casilla 653, Santiago 7800024, Chile. Tel.: +56 2 2978 7290; fax: +56 2 2271 2973.
E-mail address: m.kiwi.t@gmail.com (M. Kiwi).

0304-8853/$ - see front matter © 2013 Elsevier B.V. All rights reserved.
http://dx.doi.org/10.1016/j.jmmm.2013.02.027

alloys may display a large magnetic moment, and an important magnetocrystalline anisotropy energy (MAE). Moreover, they showed that it is possible to tailor the MAE and the magnetic moment, by adjusting the composition and the aspect ratio of the constituent elements [8]. Those predictions were ratified later by Andersson et al. [9], and are of interest because they are relevant for the recording media industry. Furthermore, Fe and Co are next to each other in the periodic table and their first neighbor distances in the bulk are very similar. Thus, they are ideal candidates to be studied within the density functional theory (DFT) approach.

Certainly, the nanosystems studied experimentally are too large for first principle calculations, but we expect that by investigating smaller structures, using *ab initio* techniques, one can obtain trends and information on the properties of these systems that lead to the understanding of the basic phenomena that are involved.

In this contribution we study $Fe_{8-N}Co_N$ nanoribbons and nanowires, varying their shape, composition and the specific arrangement of the Fe and Co atoms. To understand the basic behavior of these systems, we limit ourselves to freestanding zig-zag nanoribbons and nanowires. The properties that we investigate are their structural configurations and transformations as a function of the number N of Co atoms, and how the magnetic properties change, and compare them to the bulk properties of pristine Fe and Co and their alloys.

This paper is organized as follows: after this introduction, we present the model used and the methods of calculation in the next section. Next we present our results in two separate sections: the first deals with nanoribbons and the second with nanowires. Finally, we summarize and draw conclusions in the last section.

2. Model and methods

Our calculations were performed within the density functional theory (DFT), using plane wave basis sets as implemented in the Vienna *ab initio* simulation package (VASP) [10–13]. Since it is well known that the local density approximation (LDA) fails to reproduce the magnetic groundstate of bulk-iron, the exchange and correlation effects are described by the generalized gradient approximation (GGA) [14]. Furthermore, we used for the exchange and correlation the so-called Perdew–Burke–Ernzerhof (PBE) parametrization [15].

To calculate magnetic anisotropies an all-electron approach is necessary. In the case of VASP this is achieved by means of a frozen core full potential-projector augmented wave (PAW) method [16,17]. We used 30 k-points along the reciprocal space line (without time reversal symmetry). The plane wave cutoff was set to 300 eV, and we checked that this basis set is sufficiently large. The spin-orbit coupling in 3d metals is quite small, and does not yield any noticeable structural changes. Therefore, we performed a non-self-consistent calculation of the anisotropy, (*i.e.* keeping the atomic magnetic moment collinear to the desired axis). This approach yields the same results (within the precision reported) as fully self-consistent calculations and is several times faster. The VASP implementation of non-collinear magnetism and spin-orbit coupling was discussed in detail by Hobbs et al. [18].

Two different shapes of nanostructures were studied: zig-zag nanoribbons and nanowires. For all the geometrical structures investigated we used an eight atom supercell. This corresponds to four (two) times the periodicity of a pure zig-zag nanoribbon (nanowire). Therefore, our systems have the stoichiometry $Fe_{8-N}Co_N$. The nanowires and nanoribbons are infinite along the z-axis direction (periodic boundary conditions) and spurious transverse self-interactions are avoided by using a large vacuum space (at least 10 Å in addition to the ribbon or wire thickness).

Not only the relative concentration is important for nanoalloys but also the specific spatial atomic arrangement that the different species may adopt. This gives rise to a plethora of different 'decorations' for the same composition, the so-called *homotopes* (clusters with the same size, composition and geometrical structure, but with a different arrangement of Fe and Co atoms). In our approach, in spite of the constraint imposed by the cell size, we have a representative but tractable number of such homotopes. All the possible structures were investigated and fully optimized, including the cell height (a).

3. Results

3.1. Zig-zag nanoribbons

Zig-zag nanoribbons are among the thinnest quasi-linear systems. Their shape is quasi-2D and they have π rotational symmetry. This feature plays an important role in the orbital moment magnitude, and consequently in the magnetocrystalline anisotropy. Fig. 1 shows all the homotopes that we considered, *i.e.* all the possible Co concentrations in the unit cell. They are ordered according to their binding energy E_b: from the ground state (a) to weaker bound structures, (b), (c), etc. (see Fig. 2). By inspection of the figures it is evident that the zig-zag symmetry is preserved, at least to a large extent, for all the concentrations studied. Even more, one can see that the Fe and Co atoms are 'interchangeable'. The lowest energy structures, (a) and (b), of the $Fe_{8-N}Co_N$ nanoribbon, are equivalent to the corresponding energy states of Fe_NCo_{8-N} (for the same N value and $2 \le N \le 6$), and obtained by interchanging Fe(Co) by Co(Fe) atoms. Also, for the geometries (a)–(c) of Fe_4Co_4, the Fe and Co atoms adopt geometrically equivalent patterns. However, it is important to note that in the (b) geometry, the Fe atoms increase their bond length ($d_{Fe-Fe} = 2.61$ Å) significantly, as compared with the equivalent bond of pristine Fe nanoribbons ($d = 2.35$ Å), and the atoms are not interchangeable. Moreover, the Co–Co bond length ($d_{Co-Co} = 2.28$ Å) is nearly the same as the one of the Co_8 nanoribbon ($d_{Co-Co} = 2.26$ Å). This is due to the stronger Co–Co bonding as compared to the Fe–Fe one.

As the number of Fe and Co atoms becomes similar, the Fe and Co atoms prefer to form Fe–Co zig-zag patterns, reducing as much as possible Fe–Fe or Co–Co neighbors. Those pairs are mainly formed on top of each other. Conversely, the arrangements with the weakest binding energy are those where the Fe and Co atoms segregate, forming blocks. Actually, their binding energy is slightly lower than the arrangements in which one (or two) columns are composed of a single element.

Nonetheless, all the arrangements with the same stoichiometry have similar binding energies (see Fig. 2, upper panel), with differences of only ~ 0.03 eV/atom between the groundstate and the highest energy isotope, which is of the order of magnitude of 300 K. Therefore, a mixture of all the homotopes is likely to be found in experiments at room temperature. The energies are mainly determined by the ratio of the number of Fe and Co atoms, and the binding is stronger for a large number of Co atoms. It approximately obeys the linear relation $E_b = -0.047N - 2.67$, where $N \in [0,8]$ is the number of Co atoms, and the binding energy E_b is given in eV/atom.

The average magnetic moment of these nanowires

$$\overline{\mu} = \frac{1}{M}\sum_i \mu_i \tag{1}$$

where the sum runs over all the Co and Fe atoms located at site i in the unit cell and M is the total number of atoms in the cell, is

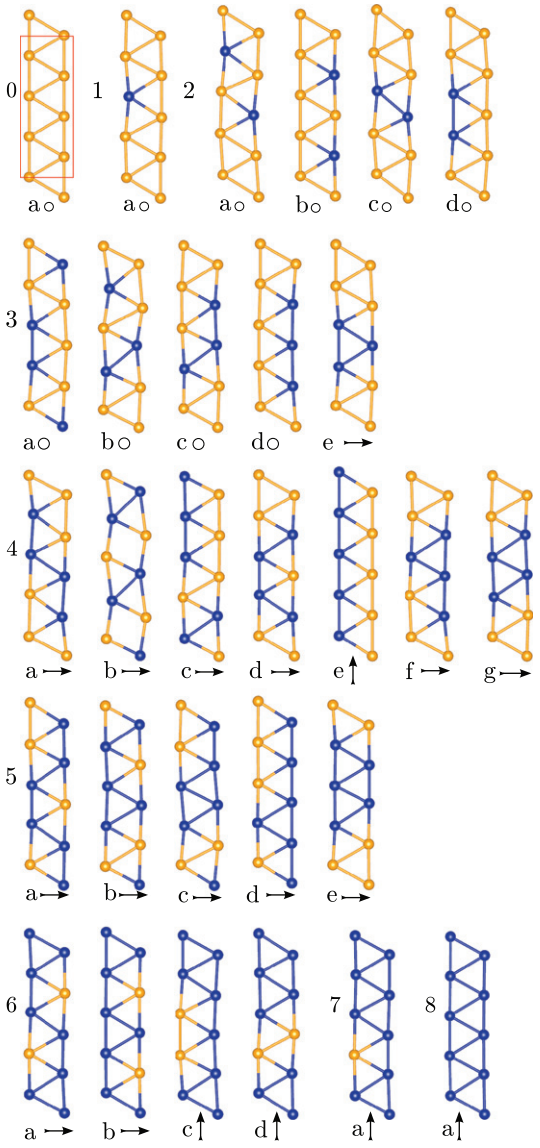

Fig. 1. Homotopes of $Fe_{8-N}Co_N$ with zig-zag nanoribbon structure. They are labeled in order of decreasing binding energy E_b, starting from the groundstate (a). Yellow and blue spheres correspond to the Fe and Co atomic positions, respectively. Bonds are drawn only if the inter-atomic distance is less than 2.6 Å, to enhance the visualization of dimerization effects. The unit cell is drawn in the upper left (pure Fe) structure. The first and last row of atoms are repeated to facilitate the visualization of the periodicity. The circles and arrows indicate the direction of the easy magnetization axis, perpendicular to the ribbon plane (circles), and parallel to that plane and parallel to the *z*-axis (arrows). (For interpretation of the references to color in this figure caption, the reader is referred to the web version of this article.)

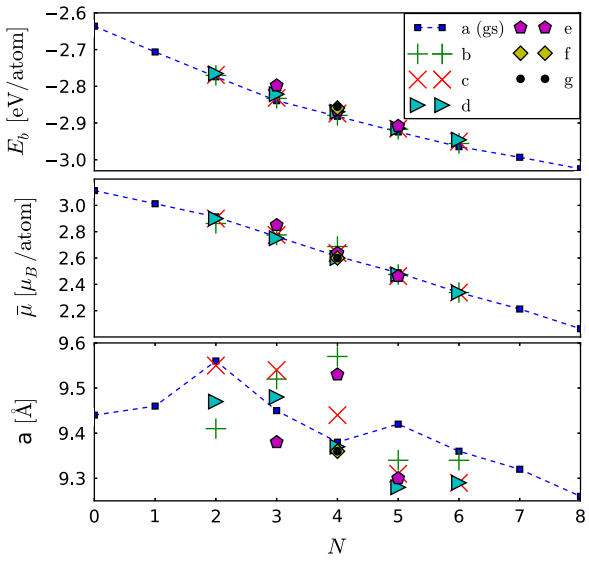

Fig. 2. The upper, middle and lower panels show the binding energy E_b, average magnetic moment $\overline{\mu}$, and height *a* of the simulation unit cell (after geometrical optimization), respectively. For every number of Co atoms ($0 \le N \le 8$) all the possible arrangements were studied. They are displayed, ordered from the groundstate to lower binding energy structures, according to the same labeling as in Fig. 1.

displayed in the middle panel of Fig. 2. As expected in these low dimensional systems, $\overline{\mu}$ is quite large, and for the pure Fe zig-zag nanowires, agrees with previous reports [19]. Remarkably, despite to the fact that the magnetic moment of each atom depends on the element and its neighborhood, the average magnetic moment is almost independent of the specific atomic arrangement and approximately obeys the linear relation $\overline{\mu}(N) = -0.134N + 3.16$, where $\overline{\mu}(N)$ is given in units of Bohr magnetons μ_B. The rate of change of $\overline{\mu}(N)$, when Fe is substituted by Co, is of the order of $1\mu_B$. This is expected due to the fact that Co contributes with one more *d* electron.

An additional feature of interest for these systems is the magnetocrystalline anisotropy energy (MAE), which corresponds to the energy difference for different magnetization directions. For the case at hand – nanoribbons and nanocylinders – we can distinguish two main directions: axial and transverse, the latter being a plane orthogonal to the *z*-axis. One can define the MAE as

$$E = E_0 + \sin^2(\theta)(K_1 + K_2\cos^2(\phi)), \tag{2}$$

where θ is the angle that forms the magnetization with the *z*-axis (NW axis) and ϕ is the azimuthal angle in the *xy* plane. The anisotropy constant $K_1 = E_{min,perp} - E_{axial}$ is the axial contribution; a positive value means that the easy axis is along the nanoribbons axis and a negative one is obtained when the easy axis lies in the perpendicular plane. K_2 is the difference between the maximum and minimum values of $E(\pi/2,\phi)$ as one sweeps the magnetization on the *xy* plane.

In Fig. 3, the upper panel provides the values for K_1. Only for $N=7$ and 8 it is positive; *i.e.* the easy axis lies along the *z*-direction. Otherwise, the easy axis lies on the plane perpendicular to the ribbon; either parallel or perpendicular to the ribbon plane. We show, in the middle panel of Fig. 3, the values of K_2. Positive values correspond to an easy axis pointing perpendicular to the ribbon plane, and correspond to $N=0$, 1, 2 and 3. On the other hand, for $N=4$, 5 and 6, the easy axis points along the ribbon plane and perpendicular to the *z*-axis. Thus, pristine Fe nanoribbons have an easy axis orthogonal to the ribbon plane (in agreement with the results of Tung and Guo [19]), and the Co nanoribbon has an axial easy axis. In both cases there is an important transverse anisotropy.

As expected, alloyed nanoribbons display a behavior that depends on the specific atomic arrangement, since a lowering of the crystal symmetry enhances the anisotropy. Despite these differences the homotopes have a linear-like dependence of the MAE as a function of *N* (the number of Co atoms). For example, regardless the Fe–Co arrangement, we obtain an Fe-like anisotropy up to $N=3$, and a Co-like anisotropy for $N=7$ and 8, while in the remaining cases the easy axis direction does depend on the structure. To understand the MAE behavior it is useful to look at the orbital magnetic moments (Fig. 3, lower panel), since for a pristine Fe nanowire the largest contribution corresponds to the magnetization perpendicular to the ribbon plane, while for a Co nanowire the largest component is along the axial axis. In the

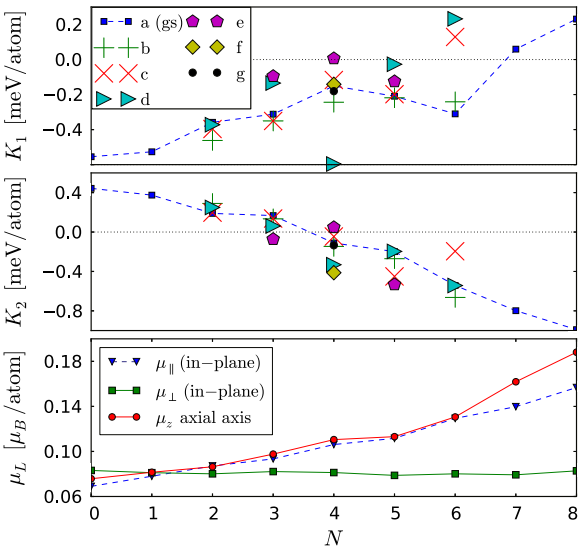

Fig. 3. The upper and middle panels illustrate the axial (K_1) and transverse (K_2) magnetocrystalline anisotropy energy, respectively, while the lower one provides the orbital magnetic moment per atom μ_L. They are given as a function of the number N of Co atoms of the zig-zag configurations illustrated in Fig. 1. $\mu_\parallel$ and $\mu_\perp$ are the orbital magnetic moment components parallel and orthogonal to the ribbon, in a plane transverse to the ribbon.

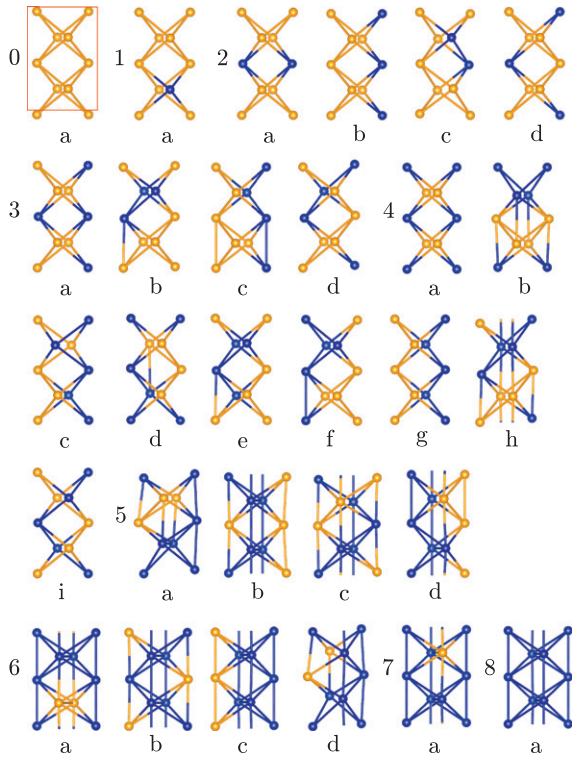

Fig. 4. Homotopes of $Fe_{8-N}Co_N$ nanowire structures, for $0 \le N \le 8$. They are labeled, from left to right, starting from the groundstate (a) and ordered in decreasing binding energy. The yellow and blue spheres indicate the Fe and Co atomic positions, respectively. Bonds are drawn only if the inter-atomic distance is less than 2.6 Å, to enhance the visualization of dimerization effects. The unit cell is drawn for the upper left (pure Fe) structure. For each structure, the two topmost atoms are repeated in the last row to facilitate the visualization of the periodicity. (For interpretation of the references to color in this figure caption, the reader is referred to the web version of this article.)

alloyed cases, there is a steady increase with N of the orbital moment along both orthogonal directions transverse to the ribbon plane, $\mu_\parallel$ and $\mu_\perp$, but the moment perpendicular to the ribbon plane stagnates, while the axial component μ_z increases steadily. This behavior helps to understand the MAE, which, for small N values, aligns the easy axis in the transverse plane direction, and only when $N \ge 7$ is reached $\mu_z \ge \mu_\parallel$, which flops the easy axis parallel to the axial axis.

3.2. Nanowires

Nanowires have a finite spatial extension in the plane transverse to the symmetry axis, and therefore a larger number of nearest neighbors than nanoribbons. Thus, they are more stable than nanoribbons, at least when they are freestanding.

The nanowire structures obtained, after a full geometrical optimization, are displayed in Fig. 4. It is quite apparent that the features found here differ strongly from the ones obtained for the zig-zag nanoribbons. The first salient feature is that the Fe and Co atoms no longer are "interchangeable". In addition, the pristine Fe and Co nanowires have a different geometry: while the former has a bcc periodicity, the latter is quasi-hcp. In essence, in spite of the small diameter size, both Fe and Co tend to adopt their bulk structures. Moreover, the low temperature bulk structure of FeCo is an ordered bcc phase, with Fe–Co first neighbors. This is the same ordering that we find for the groundstate of the $N=2$ and 4, and for nanowires, as illustrated in Fig. 4.

It is also important to notice that as the number N of Co atoms increases dimerization effects start to appear. For example, for Fe_5Co_3(b) and (c) it is apparent that some distances along the axial direction decrease, to allow for a shorter Co–Co bonding distance. In the series Fe_4Co_4 dimerization effects are more evident for some structures, like (b), which is very different from the FeCo bulk, but due to its lower dimensionality it is capable to fully dimerize and to adopt a configuration almost as favorable as the putative groundstate, labeled as (a). For $N=5$, the optimization of the number and distance of Co–Co bonds, yields an hcp-like structure while the bcc-like structure is completely absent.

An illustration of the differences and similarities between the bcc (which corresponds to the top-left 0a structure of Fig. 4), and the hcp (bottom-right 8a structure of Fig. 4) is provided in Fig. 5. For the bcc arrangement d_2/d_1 differs from the bulk value $\sqrt{3}/2$ by just 0.2%, while the angles α_1 and α_2 are also quite close to 70.52°. The hcp planes on the right of the figure are colored differently, and again the angles are almost equal to those of an equilateral triangle, namely 60°.

In Fig. 6 the nearest neighbor interatomic distances are displayed for the groundstate configurations, labeled as (a), and also for the higher energy ones. The same characteristics mentioned above are reinforced by the inspection of the numerical data. A pronounced change in the interatomic distances in the region between $N=5$ and 6 is observed, which is most notorious in the axial direction, but also noticeable in the transverse one. The interatomic distances in the oblique directions are less altered, but they are significantly smaller.

In contrast, the binding energies, shown in Fig. 7, follow an almost linear relation as N varies from 0 to 8, and much the same holds for the average magnetic moments. However, it is quite remarkable that they are practically the same for the ground state and the higher energy configurations. On the contrary, the bcc to hcp transition is clearly reflected in the cell height a, which shows a significant drop in the region between $N=4$ and 6.

In Fig. 8 we show the axial K_1 and transverse K_2 MAE for the nanowire configurations illustrated in Fig. 4. When compared with the nanoribbon case we notice similarities and differences. The magnitude of the transverse MAE is significantly smaller than that of the nanoribbon. On the other hand the axial MAE displays

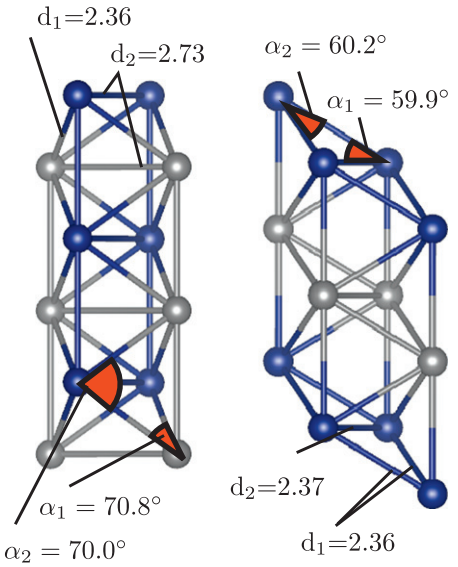

Fig. 5. Illustration of the bcc- (left) and hcp-like (right) structures the nanowire adopts as N varies from 0 to 8. They correspond to the bcc (top-left 0a structure of Fig. 4), and the hcp (bottom-right 8a structure of Fig. 4). The distances are in Å units.

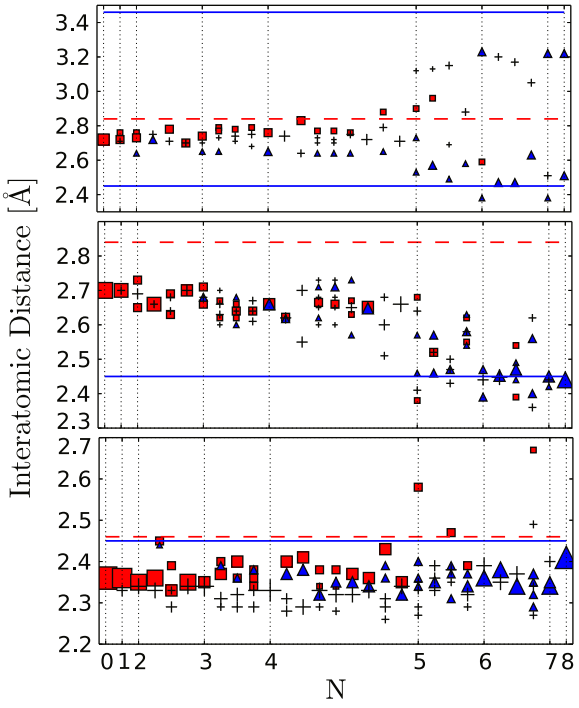

Fig. 6. Nearest neighbor interatomic distances, in Å units, in the transverse (top), axial (middle) and oblique (bottom) directions, for the $Fe_{8-N}Co_N$ nanowire structures illustrated in Fig. 4. The size of the symbols is proportional to the number of bonds of the same length (within a hundredth of an Å). The blue triangles denote the Fe–Fe, the red squares the Co–Co, and the + signs the Fe–Co interatomic distances. For a particular N value they are ordered in energy, with the groundstate (a) configuration always on the left (on the dashed lines), while the higher lying energies occupy the region between the vertical dashed lines. The horizontal dashed red (continuous blue) lines mark the bulk bcc-Fe (hcp-Co) interatomic distances. In the top graph the first and second neighbor distances of the Co hcp cell are provided. (For interpretation of the references to color in this figure caption, the reader is referred to the web version of this article.)

two sign changes; the first between $N=4$ and 5 and a second one for $N=7$. In contrast the transverse nanowire MAE is always positive indicating a magnetic moment alignment in the transverse plane. The magnitude of the three components of the

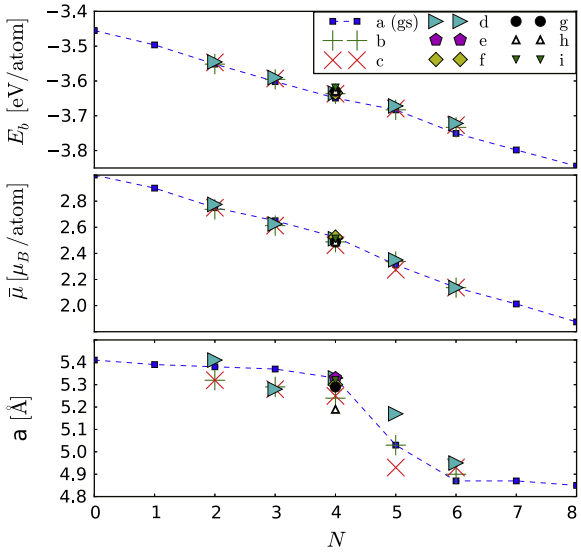

Fig. 7. The upper, middle, and lower panels show the binding energy E_b, the average magnetic moment $\overline{\mu}$, and height a of the simulation cell (after geometrical optimization), of Fe_NCo_{8-N} nanowire structures, respectively. For each number of Co atoms ($0 \le N \le 8$) all the possible nanowire arrangements were examined. They are displayed, for the groundstate (blue squares) and also for the excited state structures.

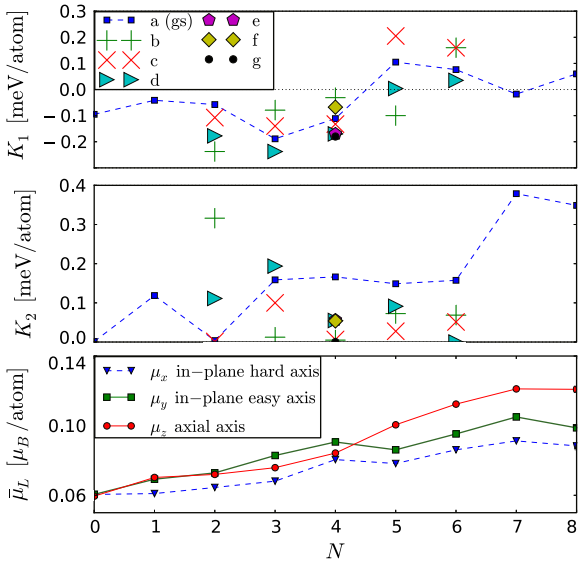

Fig. 8. The upper and middle panels the axial K_1 and transverse K_2 magnetocrystalline anisotropy energy, respectively. The lower panel provides the average orbital magnetic moment $\overline{\mu}_L$. They are given as a function of the number N of Co atoms of the $Fe_{8-N}Co_N$ nanowire configurations illustrated in Fig. 4.

nanowire orbital magnetic moment μ_L is quasi-linear functions of N, in contrast with the nanoribbon, case where one of the components hardly depends on N (see Fig. 3).

4. Conclusions

We reported above on the results of an *ab initio* calculation of the physical properties of Fe_NCo_{8-N} nanoribbons and nanowires. Different shapes and specific atomic arrangements of Fe and Co isotopes were compared. We focused our attention on the structural configurations and transformations that occur when

the number of Co atoms N is varied. Both the zig-zag nanoribbons and the nanowires exhibit a tendency to form Fe–Co bonds, which makes segregation of the Fe and Co atoms energetically unfavorable. It is quite remarkable that, even in these nanosystems, a transition from bcc Fe to hcp Co is observed, as the number N of Fe atoms decreases.

The magnetic properties show an important dependence on the Co concentration N. The magnetic easy axes may point along the three perpendicular directions depending on N. This feature may be important to tailor specific applications.

Acknowledgments

Supported by the *Fondo Nacional de Investigaciones Científicas y Tecnológicas* (FONDECYT, Chile) under Grants 11110510 (FM), 1120356 (DA), 1090225 and 1120399 (MK), and *Financiamiento Basal para Centros Científicos y Tecnológicos de Excelencia* and Grant ICM P10-061F from FIC-NINECON. J.L. Morán-López acknowledges financial support from CONACYT (Mexico) through Grant 61417. Interesting discussions with K. Nielsch and D. Görlitz are gratefully acknowledged.

References

[1] G. Prinz, Science 282 (1998) 1660.
[2] S.E. Lambert, I.L. Saunders, A.M. Patlach, M.T. Krounbi, S.K. Hetzler, Journal of Applied Physics 69 (1991) 4724.
[3] C.A. Ross, Annual Review of Materials Research 31 (2001) 203.
[4] M.K.O. Kopp, M. Lelonek, Journal of Physical Chemistry C (2001) 203–250.
[5] R. Skomski, H. Zeng, M. Zheng, D.J. Sellmyer, Physical Review B 62 (2000) 3900.
[6] S. Shingubara, Journal of Nanoparticle Research 5 (2003) 17.
[7] J.P. Pierce, E.W. Plummer, J. Shen, Applied Physics Letters 81 (2002) 1890.
[8] T. Burkert, L. Nordström, O. Eriksson, O. Heinonen, Physical Review Letters 93 (2004). ISSN 0031-9007, URL: 〈http://link.aps.org/doi/10.1103/PhysRevLett.93.027203〉.
[9] G. Andersson, T. Burkert, P. Warnicke, M. Björck, B. Sanyal, C. Chacon, C. Zlotea, L. Nordström, P. Nordblad, O. Eriksson, Physical Review Letters 96 (2006) 037205. ISSN 0031-9007, URL: 〈http://link.aps.org/doi/10.1103/PhysRevLett.96.037205〉.
[10] G. Kresse, J. Hafner, Physical Review B 47 (1993) 558.
[11] G. Kresse, J. Hafner, Physical Review B 49 (1994) 14251.
[12] G. Kresse, J. Furthmüller, Journal of Computational Materials Science 6 (1996) 15.
[13] G. Kresse, J. Furthmüller, Physical Review B 54 (1996) 11169.
[14] J.M. MacLaren, D.P. Clougherty, R.C. Albers, Physical Review B 42 (1990) 3205. 〈http://link.aps.org/doi/10.1103/PhysRevB.42.3205〉.
[15] J. Perdew, K. Burke, M. Ernzerhof, Physical Review Letters 77 (1996) 3865.
[16] P. Blöchl, Physical Review B 50 (1994) 17953.
[17] G. Kresse, D. Joubert, Physical Review B 59 (1999) 1758.
[18] D. Hobbs, G. Kresse, J. Hafner, Physical Review B 62 (2000) 11556.
[19] J. Tung, G. Guo, Phys. Rev. B 76 (2007) 094413.